OPEN ACCESS

KING'S College LONDON

King's Research Portal

DOI:
10.1109/TBME.2016.2593518

Document Version
Publisher's PDF, also known as Version of record

Link to publication record in King's Research Portal

Citation for published version (APA):
Rivolo, S., Patterson, T., Asrress, K. N., Marber, M., Redwood, S., Smith, N. P., & Lee, J. (2017). Accurate and Standardized Coronary Wave Intensity Analysis. *IEEE Transactions on Biomedical Engineering*, *64*(5), 1187-1196. [7530884]. https://doi.org/10.1109/TBME.2016.2593518

Citing this paper
Please note that where the full-text provided on King's Research Portal is the Author Accepted Manuscript or Post-Print version this may differ from the final Published version. If citing, it is advised that you check and use the publisher's definitive version for pagination, volume/issue, and date of publication details. And where the final published version is provided on the Research Portal, if citing you are again advised to check the publisher's website for any subsequent corrections.

General rights
Copyright and moral rights for the publications made accessible in the Research Portal are retained by the authors and/or other copyright owners and it is a condition of accessing publications that users recognize and abide by the legal requirements associated with these rights.

•Users may download and print one copy of any publication from the Research Portal for the purpose of private study or research.
•You may not further distribute the material or use it for any profit-making activity or commercial gain
•You may freely distribute the URL identifying the publication in the Research Portal

Take down policy
If you believe that this document breaches copyright please contact librarypure@kcl.ac.uk providing details, and we will remove access to the work immediately and investigate your claim.

Download date: 06. May. 2023

Accurate and Standardized Coronary Wave Intensity Analysis

Simone Rivolo*, Tiffany Patterson, Kaleab N. Asrress, Michael Marber, Simon Redwood, Nicolas P. Smith, and Jack Lee*

Abstract*—*Objective: **Coronary wave intensity analysis (cWIA) has increasingly been applied in the clinical research setting to distinguish between the proximal and distal mechanical influences on coronary blood flow. Recently, a cWIA-derived clinical index demonstrated prognostic value in predicting functional recovery post-myocardial infarction. Nevertheless, the known operator dependence of the cWIA metrics currently hampers its routine application in clinical practice. Specifically, it was recently demonstrated that the cWIA metrics are highly dependent on the chosen Savitzky–Golay filter parameters used to smooth the acquired traces. Therefore, a novel method to make cWIA standardized and automatic was proposed and evaluated *in vivo*. *Methods:* The novel approach combines an adaptive Savitzky–Golay filter with high-order central finite differencing after ensemble-averaging the acquired waveforms. Its accuracy was assessed using *in vivo* human data. The proposed approach was then modified to automatically perform beatwise cWIA. Finally, the feasibility (accuracy and robustness) of the method was evaluated. *Results:* The automatic cWIA algorithm provided satisfactory accuracy under a wide range of noise scenarios ($\leq$10% and $\leq$20% error in the estimation of wave areas and peaks, respectively). These results were confirmed when beat-by-beat cWIA was performed. *Conclusion:* An accurate, standardized, and automated cWIA was developed. Moreover, the feasibility of beatwise cWIA was demonstrated for the first time. *Significance:* The proposed algorithm provides practitioners with a standardized technique that could broaden the application of cWIA in the clinical practice as well as enabling multicenter trials. Furthermore, the demonstrated potential of beatwise cWIA opens the possibility of investigating the coronary physiology in real time.**

***Index Terms*—Adaptive Savitzky–Golay (S-G) filters, coronary vasculature, wave intensity analysis.**

I. Introduction

CORONARY wave intensity analysis (cWIA) is a time-domain wave separation technique well suited for the investigation of coronary artery hemodynamics, due to its capability to distinguish between the proximal and distal mechanical influences on coronary blood flow [1]–[3]. The clinical potential for cWIA is significant, having already contributed to our understanding of the pathophysiology of various disease processes affecting the coronary vasculature, including aortic stenosis [4] and left ventricular (LV) hypertrophy [5], as well as defined the impact of various interventions including biventricular pacing [6] and intra-aortic balloon therapy [7]. Furthermore, the application of cWIA in ischaemic heart disease has delineated the mechanisms of warm-up angina and the action of known anti-anginal agents [8], [9]. More recently, the demonstration of a prognostic benefit of cWIA in the setting of acute myocardial infarction has facilitated prediction of long-term myocardial recovery [10].

However, despite substantial data supporting its clinical utility, widespread uptake of cWIA as a potential diagnostic and prognostic tool has been hampered by both the operator-dependent nature of the acquisition process and the processing variability of the acquired traces [11]. While the former is mostly due to the challenging acquisition procedure and is difficult to standardize, the latter is likely attributable, as recently demonstrated [11], to the choice of the filter parameters at the level of preprocessing: such filters are used to smooth the acquired waveforms and strongly affect the cWIA-derived metrics, thus potentially generating wide variation during quantitative evaluation. This potential downfall not only precludes comparison between studies but also the collaboration between centers that would be necessary for full clinical validation of such a tool [11], [12].

Specifically, cWIA requires simultaneous measurements of pressure and flow velocity at a single point in a blood vessel. Following the approach commonly employed in the literature, a selection of beats of interest allows the waveforms to be ensemble averaged to remove high-frequency noise [1], [4], [5],

Manuscript received December 9, 2015; revised May 4, 2016; accepted June 22, 2016. Date of publication August 3, 2016; date of current version April 18, 2017. This work was supported by the Department of Health, via the National Institute for Health Research Comprehensive Biomedical Research Centre Award to Guy's & St. Thomas' NHS Foundation Trust in partnership with King's College London and King's College Hospital NHS Foundation Trust, and the Centre of Excellence in Medical Engineering funded by the Wellcome Trust and Engineering and Physical Sciences Research Council under Grant WT 088641/Z/09/Z. The work of S. Rivolo, N. P. Smith, and J. Lee was supported by the British Heart Foundation Centre of Research Excellence hosted at King's College under Grant BHF RE/08/003. The work of T. Patterson, M. Marber, and S. Redwood was supported by the British Heart Foundation Clinical Research Training Fellowship FS/14/11/30526. *Asterisk indicates corresponding author.*

*S. Rivolo and *J. Lee are with the Division of Imaging Science and Biomedical Engineering, King's College London (e-mail: simone.rivolo@kcl.ac.uk; jack.lee@kcl.ac.uk).

T. Patterson, K. N. Asrress, M. Marber, and S. Redwood are with the Cardiovascular Division, King's College London.

N. P. Smith is with the Faculty of Engineering, The University of Auckland.

This paper has supplementary downloadable material available at http://ieeexplore.ieee.org (File size: 1.24 MB).

Digital Object Identifier 10.1109/TBME.2016.2593518

This work is licensed under a Creative Commons Attribution 3.0 License. For more information, see http://creativecommons.org/licenses/by/3.0/

[8], [13]–[15]. The resulting signal-time derivatives, which are the sole inputs to cWIA, are commonly calculated by applying a Savitzky–Golay (S-G) filter either as a smoother or a differentiator [1], [11], [16]. However, the coronary pressure and velocity time derivatives are strongly influenced by the chosen S–G parameters (polynomial degree N and window width M) [11], significantly affecting the quantitative cWIA metrics (areas and peaks of the main waves). The overriding reason for this is the adverse handling by the S-G filter of the different timescale features characterizing the coronary velocity waveform, spanning from the relatively flat systolic plateau to the sharp early-diastolic rise [11]. Therefore, there is an urgent need to standardize cWIA analysis. Consequently, we have devised an algorithm to standardize and automate the calculation of cWIA, thus eliminating the operator-dependent nature of these measurements. The benefits of this algorithm are twofold: 1) the integration of cWIA as a tool in clinical practice, and 2) enabling cWIA research in cardiovascular multicenter clinical trials.

In a recent study using *in silico* data, we demonstrated that application of an adaptive S-G filter to the velocity waveform was capable of overcoming the limitations highlighted above by automatic selection of the optimal filter parameters pointwise (at each sampling point), thus opening up to the possibility of achieving a standardized and automated method to derive cWIA [12]. However, although essential, this early work employing an *in silico* evaluation was only a preliminary step in the development of an automatic cWIA algorithm. First, simulated traces were used both for algorithm optimization and algorithm evaluation. Second, the simulated traces exhibit different features to the *in vivo* measurements. Third, the pulse wave speed (PWS) in the automatic cWIA algorithm was derived from the simulation data; thus, the impact of real-life PWS estimation still needs to be taken into consideration. The need to overcome such limitations is fundamental for establishing a standardized cWIA tool. Therefore, the aim of this work is to evaluate the automatic cWIA algorithm in human participants *in vivo*, thus validating the technique and further realizing the potential of cWIA.

The newly developed algorithm was then adapted to perform beat-by-beat cWIA, thus skipping the ensemble-averaging step, which has never been performed before due to the strong impact that noise has on the velocity signal over a single cardiac cycle. The feasibility (robustness and accuracy) of the beat-wise cWIA was, in turn, evaluated *in vivo*. The introduction of beat-by-beat cWIA adds substantial value to the clinical utility of cWIA, enabling assessment of the transient variation of the coronary hemodynamics and consequently the cWIA metrics, in particular following drug administration [9], analysis of exercise physiology [8], or during the Valsalva maneuver [13], [14]).

II. Methods

In this section, we first describe the experimental procedure required for acquiring *in vivo* coronary hemodynamics in humans. Subsequently, the theoretical aspects underlying the proposed algorithm are briefly presented, namely the cWIA and the adaptive S-G filter. We then describe our novel algorithm for automatic cWIA calculation in detail, followed by the approach for estimating the acquisition noise and assessing the accuracy of the proposed algorithm *in vivo*. Finally, we present the steps followed to establish feasibility of beat-by-beat cWIA.

A. Experimental Procedure

Recordings from ten human subjects scheduled for percutaneous coronary intervention were used for this study. Patients had given informed consent to take part in the study approved by local ethics committee. Data acquisition was as per routine clinical protocols employed in the hospital [17]. Specifically, a standard 6F-guiding catheter was positioned in the aortic root. A dual-sensor pressure–velocity $0.014''$ intracoronary wire (Combowire, Volcano Corp, San Diego, CA, USA) [18] was then connected to the ComboMap console (Volcano Corp) and positioned at the tip of the guide. The guide was then inserted into the coronary ostium and the Combowire advanced in the target coronary artery and manipulated (by an experienced interventionist) until a good Doppler velocity trace was obtained. All signals were sampled at 200 Hz and stored on disk for offline analysis. The data were imported into the custom-made StudyManager program (Academic Medical Center, University of Amsterdam, The Netherlands), and one set of approximately ten consecutive beats were extracted for each patient and used for this study. The temporal alignment of the pressure and velocity waveforms was ensured by experiments performed on *ex-vivo* animal models that revealed a 55-ms delay between the pressure and flow velocity waveform associated with this specific measuring system [8], [13], [18]. Finally, it is important to underline that the ten selected datasets span different qualities (evaluated by an experienced clinical operator) from ideal quality achievable in the clinical settings to low quality (but still analyzable if part of a clinical study).

B. Coronary Wave Intensity Analysis

The steps commonly pursued to perform cWIA are briefly described [1], [8], [13]–[15], following the in-depth overview presented in [1]. The beats of interest are selected, and then, the pressure (p) and velocity (v) waveforms are ensemble-averaged. The time derivatives of these signals, input to the cWIA, are then calculated either by applying the S-G filter as a differentiator or combining an S-G smoothing filter with first-order forward finite differencing. After computing the time derivatives, the simultaneous forward and backward traveling waves can be separated as follows:

$$dI_{\pm} = \frac{dp_{\pm}}{dt}\frac{dv_{\pm}}{dt} = \pm\frac{1}{4\rho c}\left(\frac{dp}{dt} \pm \rho c\frac{dv}{dt}\right)^2 \tag{1}$$

where

$$dp\pm = \frac{1}{2}\left(dp \pm \rho c dv\right), \qquad dv\pm = \frac{1}{2}\left(dv \pm \frac{dp}{\rho c}\right). \tag{2}$$

$dI_{\pm}$ indicates forward and backward wave intensity, c represents the PWS, and ρ the blood density. Dividing the time increments by dt avoids the WIA dependence on the sampling time [1]. The

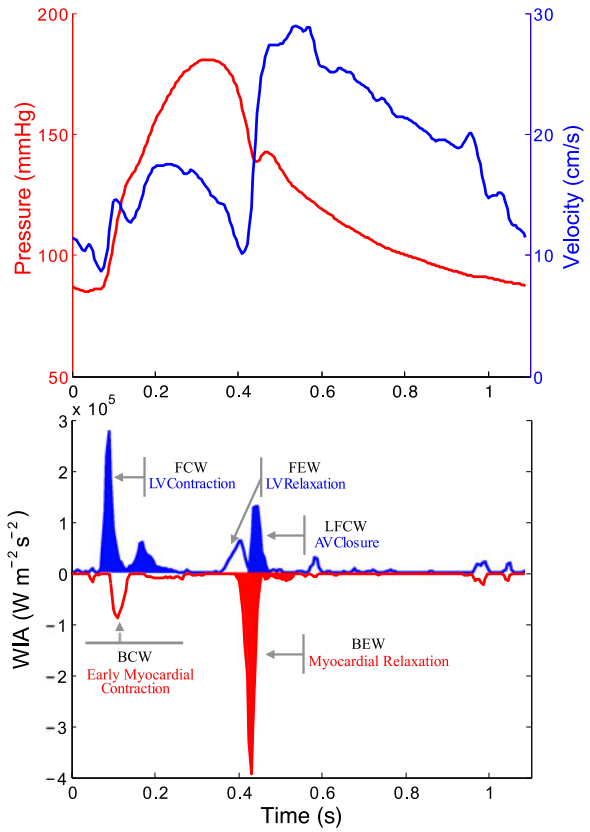

Fig. 1. *In vivo* human pressure and velocity waveform (above) along with the corresponding separated cWIA profile and the nomenclature and origin of each wave are visualized (below). The colored waves are the ones accelerating the anterograde blood flow [5], [19].

PWS is estimated by using the sum-of-squares method [1]

$$c = \frac{1}{\rho}\sqrt{\frac{\sum dp^2}{\sum dv^2}} \tag{3}$$

which is, to date, the only available method routinely applied in the coronary arteries [5], [6], [10], [15]. It is important to highlight that the summations must be performed over an integer number of cardiac periods. The cWIA-derived metrics are then defined as the integral area and peak of the main waves [5]. An example of *in vivo* human dataset with the corresponding cWIA profile, the cWIA nomenclature, and the driving mechanisms of each wave is visualized in Fig. 1. FCW, FEW, and LFCW indicate the forward compression, forward expansion, and late forward compression wave, respectively. BCW and BEW label the backward compression and backward expansion wave, respectively.

C. Adaptive S-G Filter

The S-G filters are well known and widely applied in multiple fields, from chemistry (more specifically spectrometry) to biomedical signal processing [16], [20], where the filters have been extensively described and analyzed [16], [20]–[23]. The fundamental idea of an S-G filter is to replace each noisy sample of a signal with the value of a polynomial locally fitted in a least-squares sense. More specifically, given a symmetric window around a sample point, a polynomial of degree N is fitted to the M data samples in the window [24]. However, for a local polynomial regression algorithm based on a least-squares criterion such as the S-G filter, the challenge is to find the optimal filter parameters for the regression. This problem, as shown in [24], can be solved pointwise by optimizing the Stein's unbiased risk estimator (SURE) objective [25], which is an unbiased estimator of the mean squared error. Considering the smoothing process at a sampling point n_0T, where T is the sampling time, B_{n_0} is defined as the set of samples that falls in the window width centered at n_0. The SURE risk estimator is defined as

$$\epsilon = \frac{1}{N_0}\sum_{i=1}^{N_0} f_i^2(\mathbf{x}) - \frac{2}{N_0}\sum_{i=1}^{N_0} f_i(\mathbf{x})x_i + \frac{2\sigma^2}{N_0}\sum_{i=1}^{N_0}\frac{\partial f_i(\mathbf{x})}{\partial x_i} \tag{4}$$

where N_0 is the cardinality of the set B_{n_0}, x_i are the noisy samples, and $f_i(\mathbf{x}) = \sum_{k=0}^{p} a_{k,n_0}(\mathbf{x})(nT)^k$ are the values of the fitted polynomial in the N_0 samples. The standard deviation (SD) of the noise σ is estimated using the median estimator [24]:

$$\sigma = \frac{\{\text{median}(|x_n - x_{n-1}|; n = 2, 3, \ldots, N)\}}{0.6745}. \tag{5}$$

The SURE estimator can be used to adaptively choose the window width for a fixed polynomial degree (labeled awS-G) or to adaptively choose the suitable polynomial degree for a fixed window width (labeled apS-G). In both cases, for each sampling point, the SURE ϵ cost function is calculated for each window width or polynomial degree and the one providing minimum ϵ is assumed to be optimal.

Note that, as detailed in [24], a regularization term can be added to the SURE risk estimator ϵ to improve the performance of the algorithm in regimes of low signal-to-noise ratio (SNR), which is a measure of quality of a signal (calculated as P_s/P_n, where P_s and P_n represent the power of the signal and the noise, respectively). However, this is not considered in this study due to the poorer performance exhibited by the regularized SURE risk estimator in the *in silico* analysis [12].

D. Automatic cWIA

The major steps of the newly introduced automatic cWIA are illustrated schematically in the flowchart in Fig. 2.

Initially, the selected beats of the pressure and velocity waveforms are ensemble-averaged following the standard procedure employed in the literature [1], [8], [13]–[15].

Following this averaging, the adaptive apS-G filter combined with the SURE risk estimator is applied to automatically smooth the velocity waveform. The window width is fixed at $M = 11$, following [12]. Note that the awS-G is not considered due to the lack of performance exhibited in our previous *in silico* study [12]. This will be further discussed in Section IV.

It is important to highlight that the S-G filter is used as a smoother and not as a differentiator, due of the poor performance exhibited by this second approach [11]. Moreover, based on the sensitivity analysis results described in [11], the filter is applied only to the flow velocity waveform, since it is the one most affected by noise, and the pressure trace is not smoothed.

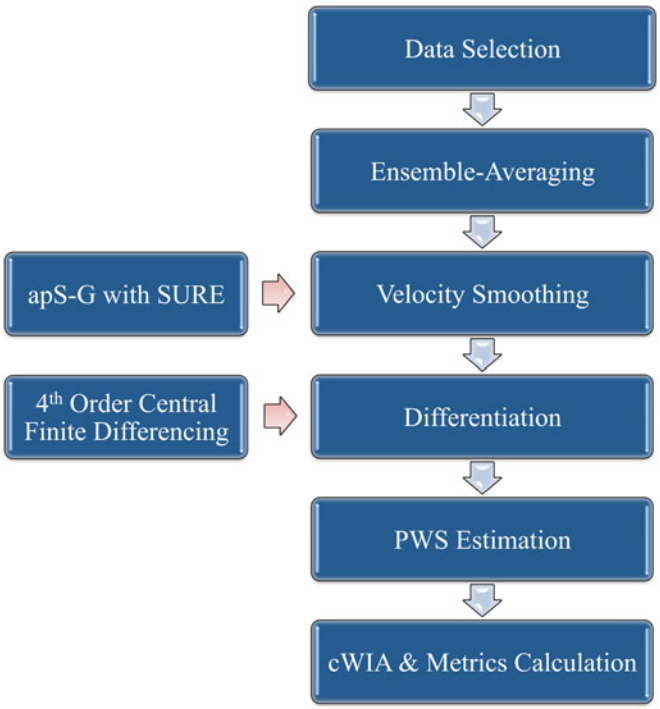

Fig. 2. Visualization of the automatic cWIA algorithm steps. Initially, the beats of interest are selected and the pressure and velocity traces are ensemble-averaged. The velocity trace is then smoothed using the apS-G algorithm combined with the SURE risk estimator. The signal time derivatives are then estimated by fourth-order central finite differencing. Finally, the cWIA is performed and the relevant metrics are calculated. The details of the choices for the velocity smoothing algorithm and for the differentiation step can be found in the text.

After the smoothing step, the time derivatives of the pressure and velocity waveform are calculated by fourth-order finite differencing [11]. Subsequently, the PWS is estimated using the sum-of-squares method and the cWIA-derived metrics are calculated, as detailed in Section II-B.

Finally, it is relevant to note that the steps introduced above can be easily adapted to exclude the ensemble-averaging step to perform beatwise cWIA.

E. Estimation of the Acquisition Noise

As detailed in the following section, the accuracy of the automatic cWIA algorithm is evaluated by adding synthetic noise to the acquired velocity waveforms. Prior to it, it is pivotal to investigate if the type of synthetic noise added resembles the noise typical of the acquisition process.

Therefore, for each dataset, the power spectrum of the acquired velocity waveform is initially calculated to assess if specific noise frequencies could be detected. The velocity trace is then ensemble-averaged and the resulting waveform subtracted from each beat to obtain an estimate of the acquisition noise. The mean and SD of the estimated noise are then calculated. Finally, multiple noise distributions are fitted to the estimated noise and compared in terms of Q–Q plot (plot of the quantiles of the estimated noise against the quantiles of the fitted distribution), P–P plot (comparing the empirical cumulative distribution function of the estimated noise with the fitted theoretical cumulative distribution function), and the root-mean-squared error (RMSE) between the empirical and fitted cumulative density functions.

F. Accuracy of the Automatic cWIA

A high-quality (evaluated by an experienced clinical operator) trace was chosen among the human datasets introduced in Section II-A and ensemble-averaged. cWIA was then applied and the calculated areas and peaks of the main waves used as gold standard. The motivation behind the use of real data as gold standard will be discussed below in Section IV.

To simulate the noise characterizing the data acquisition procedure, white Gaussian noise of zero mean and an SD varying between 5 and 30 cm/s, in steps of 5 cm/s, was added to the consecutive beats of the measured velocity profile. The choice of the type and amount of noise added is debated in Section IV. However, note that the spectrum of the noise imposed was chosen to closely represent the different scenarios typical of the clinical practice, without specific focus on the resulting SNR values. Furthermore, it is crucial to assess the algorithm's performance not only in the high-noise-level scenario but also in the low-noise-level one, since it is also required to process high-quality traces without oversmoothing them.

The automatic cWIA method (see Section II-D) was then applied, and the cWIA-derived metrics were compared with the case when zero noise was added (gold standard). The accuracy was assessed in terms of the percentage error defined as

$$\text{percentage error} = \frac{|\text{metric}_{i_{GD}} - \text{metric}_i|}{\text{metric}_{i_{GD}}} \times 100 \qquad (6)$$

where metric is the area or the peak of a specific wave, GD refers to the gold standard (zero noise added), and the index i refers to a specific cWIA waves following the common nomenclature employed in the literature [5]. The percentage error was calculated as mean $\pm$ SD, where the mean was computed over 100 experiments to account for the stochastic nature of noise.

White Gaussian noise is usually considered representative of the noise properties typical of the data acquisition [26]. To cover the more general possibility of nonsymmetric noise, the algorithm performance was also assessed for Poisson noise with the parameter $\hat{\lambda}$ varying in the range of 5–30 cm/s in steps of 5 cm/s and then repeating the protocol described above.

The protocol presented above to assess the accuracy of the proposed algorithm was then repeated for each of the other nine datasets following the exact same steps.

G. Beatwise cWIA

The feasibility and consistency of the beatwise cWIA was evaluated in two steps. First, the accuracy of the automatic cWIA algorithm was assessed repeating the pipeline described above. However, for this step, a single trace was used, since the ensemble-averaging step was not required.

Second, to assess the consistency of beat-by-beat cWIA, four datasets of approximately ten consecutive beats each were extracted from the dataset of a single patient. The cWIA algorithm was then applied to each beat and cWIA metrics were then calculated.

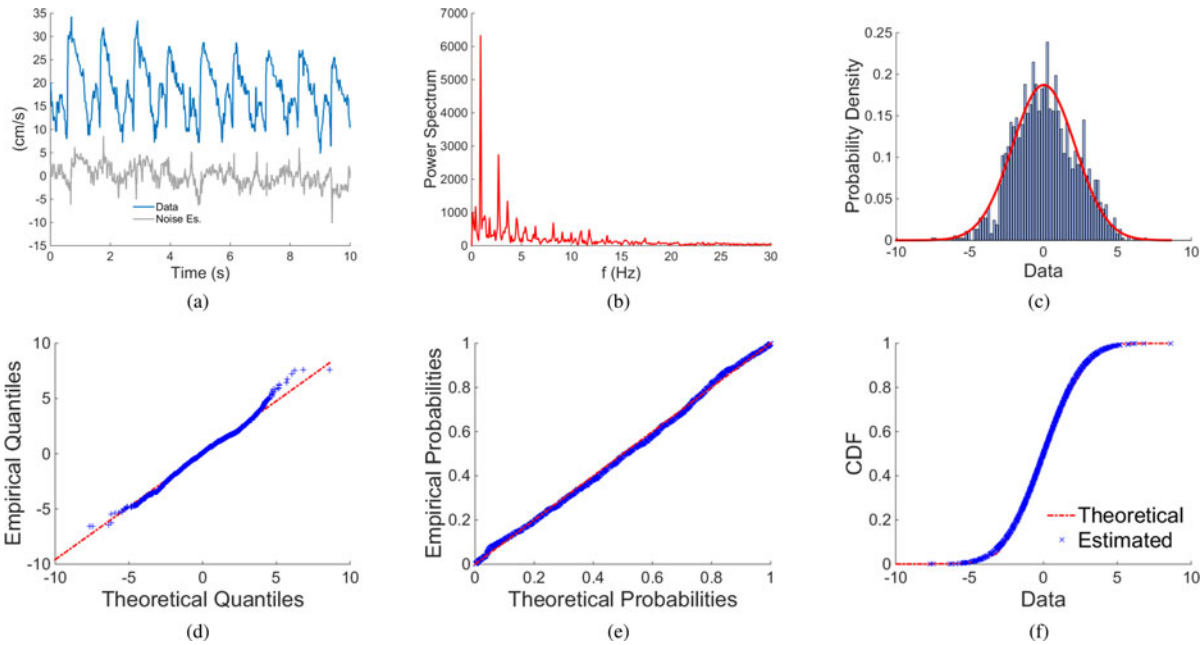

Fig. 3. (a) Example of a velocity dataset is visualized (blue) along with the estimated noise (gray), obtained by subtracting the ensemble-averaged waveform from each beat. (b) Dataset power spectrum is displayed highlighting that most of the signal information belongs to frequencies lower than 10 Hz. (c) Histogram of the estimated noise is then visualized along with the fitted Gaussian distribution (red), demonstrating that modeling the synthetic noise using white Gaussian noise (zero mean) is an adequate assumption. This is confirmed when the estimated (d) Q–Q plot, (e) P–P plot, and (f) cumulative distribution function (blue) are compared to the theoretical prediction (red) for white Gaussian noise. These results hold for all ten datasets analyzed.

III. Results

A. Estimation of the Acquisition Noise

In Fig. 3(a), the velocity trace of one dataset is visualized (blue) along with the estimated noise (gray), obtained by subtracting the ensemble-averaged waveform. As can be noticed in the corresponding power spectrum [see Fig. 3(b)], most of the signal power is concentrated in the frequencies below 5–10 Hz, making it challenging to distinguish between signal and noise.

For all the datasets analyzed, fitting a Gaussian distribution provided a satisfactory fit to the estimated noise [as visible in Fig. 3(c)] with zero mean and SD included in the range [2, 10]. This is confirmed by the Q–Q plot and P–P plot [see Fig. 3(d) and (e)], showing an approximately identity line when comparing the theoretical quantiles/probabilities with the empirical ones. Finally, the RMSE between the theoretical and estimated noise is <0.01 across all the datasets analyzed, confirming that white Gaussian noise is an adequate model to simulate synthetic noise representative of real-life scenarios.

Finally, it is important to underline that the maximal amount (SD) of the white Gaussian noise added when assessing the algorithm accuracy is three times as large as the estimated SD (<10). Furthermore, adding Poisson noise significantly overestimates the amount of noise typical of the acquisition procedure, since the Poisson distribution samples are always positive. In summary, the cWIA algorithm proposed has been tested in much higher noise scenarios than the ones suggested by the data to perform a stringent evaluation.

B. Accuracy of the Automatic cWIA

First, note that the threshold for acceptable error was set to 10% for the wave areas and 20% for the wave peaks, following two observations. First, these values are lower than the differences reported in the literature when stratifying patients or assessing the impact of a specific clinical procedure. Specifically, a variation in the investigated cWIA metric in the range of approximately 30% [4], [5], [10] up to over 50% [8], [13] has been reported when comparing two group of patients or pre- and postdrug administration. Second, it should be considered that the cWIA inputs are the time derivatives of signals, which contain an amplified level of noise than the raw signals themselves.

The automatic cWIA algorithm successfully removed most of the imposed simulated noise, as evidenced by Fig. 4. All the main waves areas were accurately estimated ($\leq$10% error) through most of the levels of noise added (SD 5–25 cm/s), as shown in Table I. Moreover, even in the case of extremely high levels of noise (SD = 30 cm/s) [see Fig. 4(c)], the algorithm performance was only slightly over the 10% accepted limit (see the last column of Table I).

The automatic cWIA algorithm was capable of adequately estimating the main wave peaks only up to a noise level of SD = 15–20 cm/s (see Table I), which is still remarkable considering the amount of simulated noise [see Fig. 4(b)]. Furthermore, it is important to highlight that the FCW and BEW (the most clinically relevant waves [3], [5]) are the most robust to the added noise when the peak accuracy is evaluated.

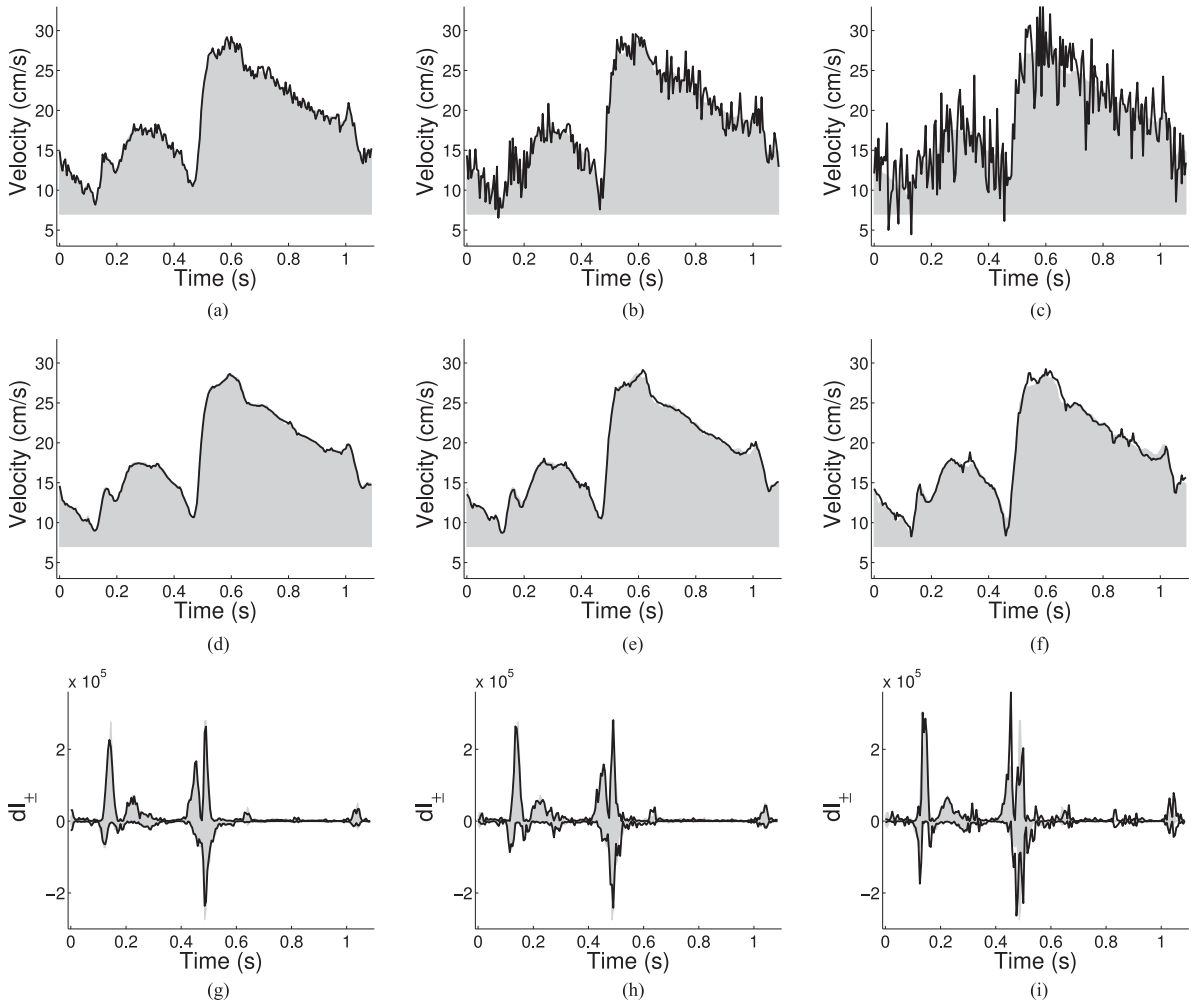

Fig. 4. Automatic cWIA algorithm results for the different levels of noise tested are highlighted. In the first row (a)–(c), the impact of the different level of noise on the velocity waveforms (solid black line) are compared to the gold standard waveform (gray shadowed). In the second row (d)–(f), the automatically denoised traces (solid black line) are compared once again with the gold standard velocity waveform, highlighting the capability of the algorithm to remove most of the simulated noise. In the last row (g)–(i), the automatically denoised cWIA profiles and the gold standard one are visualized superimposed.

TABLE I
PERCENTAGE ERROR (MEAN AND SD OVER 100 EXPERIMENTS) FOR THE AREAS AND PEAKS OF THE MAIN WAVES IS LISTED FOR THE AUTOMATIC CWIA ALGORITHM APPLIED TO THE HUMAN *In Vivo* DATASET WHEN WHITE GAUSSIAN NOISE IS ADDED

Automatic cWIA Accuracy - White Gaussian Noise						
Areas						
Noise	**SD = 5**	**SD = 10**	**SD = 15**	**SD = 20**	**SD = 25**	**SD = 30**
FCW	1.7 ± 1.4	2.8 ± 1.8	4.7 ± 4	6.4 ± 4.9	10.2 ± 7.1	11 ± 8
FEW	3.4 ± 2	4.3 ± 3.4	6.4 ± 4.7	8 ± 6.5	10.7 ± 7.9	14.1 ± 12.1
LFCW	4.1 ± 3	7.4 ± 4.8	8.7 ± 6	10 ± 6.4	13.6 ± 9.3	15.8 ± 12.7
BCW	2.5 ± 1.9	4.1 ± 2.7	7.1 ± 6	9.7 ± 6.9	13.5 ± 9.6	13.2 ± 8
BEW	1.8 ± 1.3	3.4 ± 2.5	4.4 ± 3.5	5.6 ± 4.8	8 ± 6.7	8.9 ± 6.3
Peaks						
FCW	6 ± 3.5	8.6 ± 6.1	10.3 ± 7.9	13.3 ± 12.1	20.2 ± 18	30.4 ± 25
FEW	6.9 ± 6	18.1 ± 15.7	36 ± 28.6	> 50	> 50	> 50
LFCW	9.3 ± 6	12.5 ± 9.2	13.4 ± 10	17.9 ± 15.3	22.9 ± 22.7	31.8 ± 32.1
BCW	13.8 ± 6.3	12.8 ± 10.7	12.9 ± 13.7	19.7 ± 13.5	33.5 ± 24.2	47.4 ± 42
BEW	4.8 ± 3.8	8.2 ± 5.3	9.7 ± 7	13.1 ± 15.1	15.7 ± 14.8	18.1 ± 16.1

The newly proposed algorithm also provided satisfactory accuracy even in the case of nonsymmetric noise (Poisson noise), as highlighted in Table II. More specifically, the areas and peaks of the main waves were estimated with $< 10\%$ error and $< 20\%$ error, respectively, for all the levels of noise investigated.

Finally, the average SNR reduction provided by the automatic cWIA algorithm was investigated. It is possible to see in Fig. 5 that the average improvement provided by the algorithm over 100 simulations in terms of SNR varied between 24% for the lowest level of noise and 84% for the highest level of white Gaussian noise. These results are in good agreement with those published for the original development and testing of the algorithm on *in silico* and *in vivo* ECG traces [24]. This result highlights the capability of the method to significantly improve the SNR, especially in high-noise scenarios. In the case of Poisson noise, the improvement in terms of SNR is more limited (5–10%), but the accuracy provided by the automatic cWIA algorithm remains satisfactory due to the dependence of cWIA solely on the signal's time derivatives. The results presented

TABLE II
PERCENTAGE ERROR (MEAN AND SD OVER 100 EXPERIMENTS) FOR THE AREAS AND PEAKS OF THE MAIN WAVES IS LISTED FOR THE AUTOMATIC cWIA ALGORITHM APPLIED TO THE HUMAN *In Vivo* DATASET WHEN POISSON NOISE IS ADDED

Automatic cWIA Accuracy - Poisson Noise						
Areas						
Noise	$\hat{\lambda}=\mathbf{5}$	$\hat{\lambda}=\mathbf{10}$	$\hat{\lambda}=\mathbf{15}$	$\hat{\lambda}=\mathbf{20}$	$\hat{\lambda}=\mathbf{25}$	$\hat{\lambda}=\mathbf{30}$
FCW	3.1 ± 1	3.5 ± 1.5	3.8 ± 1.8	3.6 ± 1.8	4.1 ± 1.8	4 ± 2.5
FEW	0.8 ± 0.6	1.1 ± 0.7	1.2 ± 0.9	1.4 ± 1	1.5 ± 1	1.6 ± 1.2
LFCW	8 ± 1.3	8.3 ± 1.8	8.5 ± 2.3	8.1 ± 2.6	8.7 ± 2.9	9 ± 3.7
BCW	4.9 ± 1.3	5.8 ± 2.2	6 ± 2.6	6 ± 2.5	6.7 ± 2.6	6.5 ± 3.3
BEW	4 ± 0.9	4.2 ± 1.1	4.2 ± 1.5	3.9 ± 1.5	4.3 ± 1.8	4.7 ± 2.1
Peaks						
FCW	3.7 ± 2.2	5.4 ± 2.6	5 ± 2.7	6.5 ± 3.5	7.1 ± 3.7	5.8 ± 3.7
FEW	2.3 ± 1.8	4 ± 2.4	4 ± 3.3	6.1 ± 4.7	7.3 ± 6.2	6.9 ± 6.2
LFCW	3.3 ± 2.5	7.1 ± 3.6	7.1 ± 4.4	6.9 ± 4.1	7.5 ± 5.2	8.3 ± 5.4
BCW	12.2 ± 5	13.1 ± 6.2	13.1 ± 6.7	13.4 ± 7.1	14.5 ± 7.3	14.1 ± 6.6
BEW	1.7 ± 1.4	3.8 ± 2.3	3.8 ± 2.9	4.8 ± 3.3	4.5 ± 3.6	5.5 ± 3.9

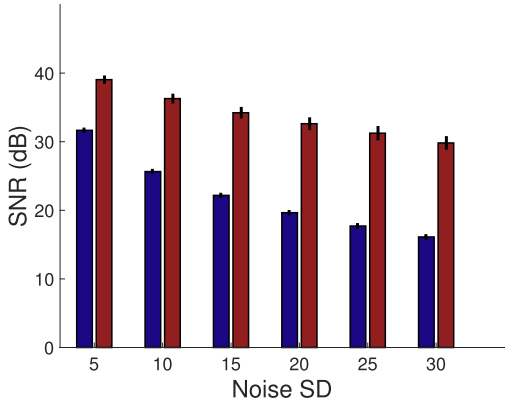

Fig. 5. SNR averaged over 100 experiments is visualized for the noisy (white Gaussian noise) signals (blue) and for the ones obtained after applying the automatic cWIA algorithm (red).

above hold quantitatively and qualitatively when the accuracy of the automatic cWIA has been tested in the other nine datasets.

C. Beatwise cWIA

The feasibility of applying the automatic cWIA algorithm on a beatwise basis was initially evaluated by repeating the *in vivo* validation performed above using a single beat (avoiding the ensemble-averaging step). The algorithm was able to successfully ($\leq 10\%$ percentage error) remove the simulated noise for SD $\leq$ 20 cm/s when the wave areas were considered. The same results were obtained for the wave peaks where an estimation error $\leq 20\%$ was achieved in the noise range of SD 5–15 cm/s. When the Poisson noise was imposed, satisfactory accuracy was obtained for all levels of noise tested when considering the waves areas and for $\hat{\lambda} < 25$ when considering the waves peaks.

Following the above analysis, our automatic cWIA approach was applied on four datasets of approximately ten beats each extracted from the same patient at baseline, but at different times in order to test the consistency of a fully automatic beat-by-beat real-time cWIA. The cWIA profile was adequately captured

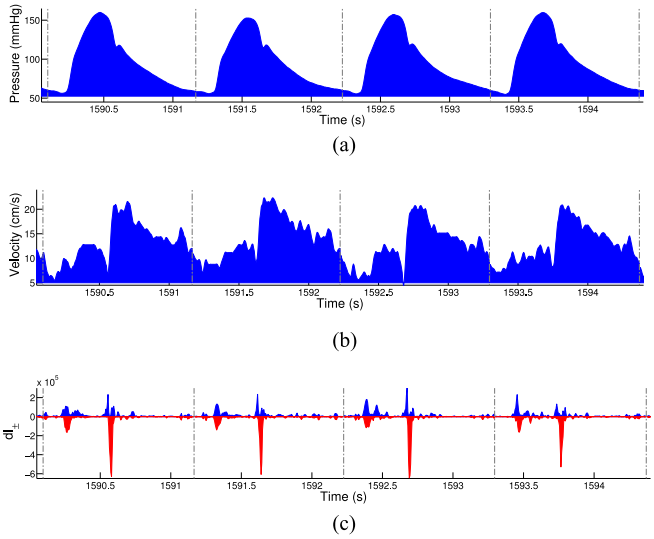

Fig. 6. Example of fully automatic beatwise cWIA on four beats is shown (c) along with the pressure (a) and velocity (b) waveforms. The apS-G filter has been applied only on the velocity waveform.

beatwise (see Fig. 6), as the main waves are easily recognizable in each beat. The percentage variation of the FCW and BEW areas was then calculated for each beat and compared with respect to the value obtained from the average of the 47 beats analyzed (belonging to four datasets taken form the same patient at different times during baseline). Most of the percentage variation was concentrated in the range $\pm 25\%$; however, there were values up to $\pm 50\%$, especially if the FCW is of interest [see Fig. 7(a)]. This percentage variation can be partially ascribed to the fluctuations in the beatwise estimated PWS since, as shown in Fig. 7(c), this value varied in the range $\pm 40\%$, where the main wave areas were shown to be sensitive to an error in the PWS estimation [14]. However, the beatwise values of the FCW and BEW areas and peaks compared well with those presented in [5]. Moreover, the percentage of the FCW and BEW area over the total wave energy (total integral area of $dI_{\pm}$) was remarkably consistent through all of the different beats [see Fig. 7(b)] and the beat-by-beat variations did not impact the possibility of distinguishing between the two waves contributions (p-value $<$ 0.001).

Finally, if real-time cWIA is of interest, the developed automatic pipeline needs to have low compute times. The average time to perform both the apS-G and awS-G algorithms for both the SURE and rSURE risk estimator on a single beat was 0.06 $\pm$ 0.003 s on a standard desktop computer using an unoptimized MATLAB code (MATLAB 2014b, The MathWorks, Inc., Natick, MA, USA). No specific effort was made to optimize the algorithm since the computational speed is already suitable for real-time cWIA.

IV. DISCUSSION

Before a discussion about the different aspects of this paper, it is important to recall the main goal of this study. As mentioned in Section I, the widespread uptake of cWIA in the clinical settings has been hampered by the known variability of the

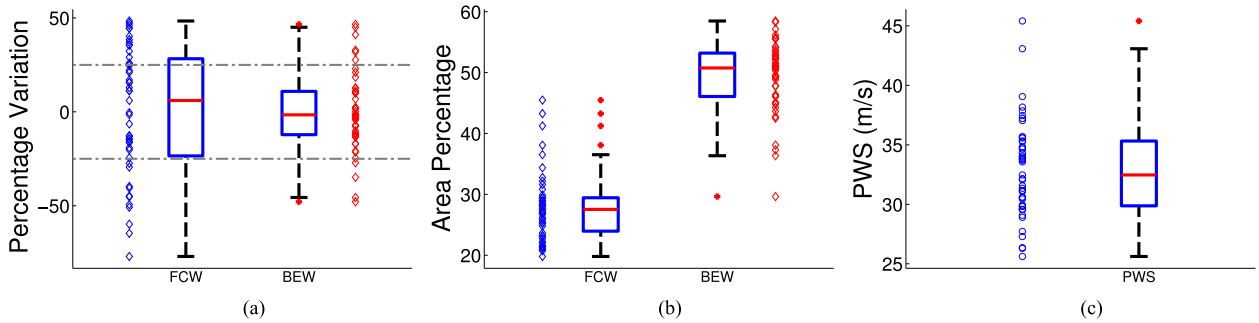

Fig. 7. (a) Percentage variation of the FCW and BEW areas over the 47 beats analyzed with respect to the averaged value is visualized. The gray horizontal lines mark the $\pm 25\%$. (b) Area percentage occupied by the FCW and BEW with respect to the total wave energy over each cardiac cycle is presented. The contribution of the investigated waves is consistent through the processed beats and significantly different (p-value < 0.001). (c) PWS estimated using the sum-of-squares method for each beat is highlighted.

cWIA metrics to both the acquisition procedure and the signal processing.

The former derives from the challenge of obtaining a stable Doppler flow envelope, which requires a subtle but continuous tuning (translation and rotation) of the catheter tip. This clearly makes the acquired flow velocity operator dependent. However, it is important to underline that the acquisition is performed by highly specialized interventionists to obtain the highest quality velocity trace, thus reducing this dependence.

Concerning the processing variability, it has been recently demonstrated that the choice of the S-G filter parameters, usually employed to smooth the acquired signals [1], [5], has a strong impact on the cWIA-metrics [11]. Therefore, the aim of this study is to achieve operator independence of the postprocessing technique based on a well-defined objective criterion of optimality.

A. Noise Estimation

The noise estimation has been performed by subtracting the ensemble-averaged waveform to each of the acquired beats, thus assuming that the ensemble-averaged trace closely represents the noise-free data. Note that this assumption is typically considered valid if the same exact event (in our case a cardiac cycle) is measured multiple times, since the randomness of the acquisition noise would affect each measurement in a different way. However, the acquisition procedure is challenging due to the cardiac motion and enables only a limited amount of beats to be measured consecutively (typically 10–15), after which the catheter has to be repositioned. Therefore, the noise estimation performed in this study by averaging over approximately ten beats is the best option available with the current technology.

Finally, it is important to discuss the choice of assessing the accuracy of the newly proposed approach by adding synthetic noise to real data. This is motivated by multiple reasons. First, there is a lack of gold standard techniques to perform cWIA to compare to the new proposed method [11]. Furthermore, ground-truth data for testing the newly introduced approach are not available in the literature. Finally, it will be difficult to evaluate the accuracy of the automatic cWIA by applying it on multiple *in vivo* datasets and then comparing the obtained cWIA metrics with the literature values, due to the significant variability reported [5], [6], [8], [13]–[15], [27]. For these reasons, adding different types and ranges of synthetic noise on high-quality data (minimal acquisition noise) provides a controlled experimental setup, closely reproducing the most typical clinical scenarios, where the accuracy of the new proposed method could be assessed. Moreover, the amount of noise added is significantly higher than the amount estimated from the data, thus subjecting the proposed algorithm to a severe test when assessing the accuracy.

Nevertheless, the result of applying the automatic cWIA algorithm on each of the ten acquired datasets is demonstrated in the online supplementary material for sake of completeness.

B. Accuracy

The accuracy of the new approach was assessed in terms of the cWIA-derived clinically relevant metrics, which are the areas and peaks of the main waves [5], [8], [10]. The *in vivo* analysis confirmed qualitatively and quantitatively the findings of the *in silico* study [12]. The main wave areas were accurately calculated ($\leq$10%) for most of the noise scenarios investigated (see Tables I and II). This is quite remarkable since the amount of noise imposed on the velocity waveform was approximately doubled in comparison to the previous *in silico* analysis [12]. Moreover, the PWS had to be estimated using the sum-of-squares method possibly adding a significant source of variability, due to the sensitivity of the cWIA metrics with respect to an error in the PWS estimation [11], [14]. The maximum level of noise tested increased the percentage error up to 15%, which is still acceptable particularly in view of the excessive amount of noise simulated [see Fig. 4(c)]. In terms of the wave peaks (as used in some studies [10]), the proposed approach still provided high levels accuracy for low and medium levels of noise. However, it is important to highlight that the area of the main waves should be preferred as a clinical metric compared to the wave peaks, since it exhibited higher robustness to noise in our analysis.

C. Parameter Choice and Robustness

As described in Section II-D, the proposed algorithm utilizes the apS-G filter with the SURE risk estimator to automatically select at each sampling point the optimal polynomial degree

for smoothing the velocity waveform. This choice follows the results obtained in the *in silico* analysis [12], since the awS-G (automatic selection of the optimal window width M) exhibited strong dependence on the prefixed polynomial degree [12]. Similar conclusions have been obtained when comparing in preliminary tests the awS-G and apS-G with the SURE risk estimator using the *in vivo* data.

Finally, although not shown in detail, it is important to underline that in order to evaluate the robustness of the proposed algorithm *in vivo* the accuracy of the automatic cWIA has been evaluated for multiple pre-fixed polynomial degree ($M =$ [9 11 13 15]) following exactly the same protocol illustrated in Section II-F. Similar accuracy was obtained thus confirming *in vivo* the robustness of the algorithm previously observed in the *in silico* study [11].

D. Real-Time Beatwise cWIA

When the automatic cWIA algorithm was applied on a single trace, the results were satisfactory in the low- and medium-noise regime (see Section III-C). A higher level of noise impacted the cWIA profile especially when the FEW and LFCW were considered. This is probably due to the close temporal proximity of the two waves. However, these results demonstrated the feasibility of a real-time cWIA and motivated the need to verify the consistency of the new approach.

This was achieved using multiple beats selected in the same patient. Comparing the FCW and BEW areas of four different datasets extracted from the same patient hemodynamics demonstrated that the beatwise variability with respect to the metric averaged value was mostly confined to the $\pm 25\%$ range when the BEW was investigated [see Fig. 7(a)]. Furthermore, the consistency of the FCW and BEW percentage area with respect to the total wave energy was higher than the waves' specific values [see Fig. 7(b)]. This is noteworthy since the beatwise PWS estimation provided by the sum-of-squares method varied up to 80%, thus strongly affecting the beatwise values of the cWIA metrics, due to their strong dependence on variations in the estimated PWS larger than 40% [11], [14]. Furthermore, as previously highlighted, beatwise cWIA is a novel application, therefore hard to compare with the available literature.

It is important to underline the beneficial impact that real-time beatwise cWIA could have on the coronary physiology research settings. When applying cWIA to investigate the impact a specific vasodilator [9], exercise [8], or Valsalva manoeuvre may have on the coronary hemodynamics, currently only the initial (baseline) and final states are assessed, since ensemble-averaging is needed thus fully ignoring the transient changes. However, this transient phase could also be rich in physiological information. For instance, it could be of great interest to evaluate the temporal delay between the infusion of a drug and its full effect, to optimize its administration, or to track on a beat-by-beat basis the changes in coronary flow patterns during exercise, thus investigating the patient-specific trajectories. The developed beatwise cWIA makes these applications possible for the first time.

E. Conclusion

In this paper, a new approach making cWIA standardized and fully automated was presented. This was achieved combining ensemble-averaging and high-order central finite differencing with the apS-G algorithm with the SURE risk estimator, with fixed window width $M = 11$.

The robustness and accuracy of the proposed algorithm were thoroughly tested by means of *in vivo* data for different levels of noise, representative of clinically observed values. The algorithm provided an error in the wave areas and peaks estimation of $\leq 10\%$ and $\leq 20\%$ in most of the simulated noise scenarios (see Fig. 4).

This novel method enables the application of cWIA on a beat-by-beat basis for the first time. Real-time beatwise cWIA was demonstrated to be consistent between consecutive heart beats.

From these results, two main conclusions with a strong clinical impact can be drawn. On one hand, the automatic cWIA algorithm provides an accurate and standardized method to perform cWIA in the clinic, removing the operator bias from the analysis and consequently favoring the widening of cWIA in the clinical practice. On the other hand, the demonstrated potential of beatwise cWIA opens the possibility of investigating the coronary physiology in real time.

The code will be made available on http://www.havmgroup.com/tools.

References

[1] K. H. Parker, "An introduction to wave intensity analysis," *Med. Biol. Eng. Comput.*, vol. 47, no. 2, pp. 175–188, 2009.

[2] J. Lee and N. P. Smith, "The multi-scale modelling of coronary blood flow," *Ann. Biomed. Eng.*, vol. 40, pp. 1–15, 2012. [Online]. Available: http://dx.doi.org/10.1007/s10439-012-0583-7.

[3] S. Sen *et al.*, "Wave intensity analysis in the human coronary circulation in health and disease," *Current Cardiol. Rev.*, vol. 10, pp. 17–23, May 2013.

[4] J. E. Davies *et al.*, "Arterial pulse wave dynamics after percutaneous aortic valve replacement: Fall in coronary diastolic suction with increasing heart rate as a basis for angina symptoms in aortic stenosis," *Circulation*, vol. 124, no. 14, pp. 1565–1572, Oct. 2011.

[5] J. E. Davies *et al.*, "Evidence of a dominant backward-propagating "suction" wave responsible for diastolic coronary filling in humans, attenuated in left ventricular hypertrophy," *Circulation*, vol. 113, no. 14, pp. 1768–1778, Apr. 2006.

[6] A. Kyriacou *et al.*, "Improvement in coronary blood flow velocity with acute biventricular pacing is predominantly due to an increase in a diastolic backward-travelling decompression (suction) wave," *Circulation*, vol. 126, pp. 1334–1344, Aug. 2012.

[7] K. De Silva *et al.*, "Coronary and microvascular physiology during intra-aortic balloon counterpulsation," *JACC Cardiovascular Interventions*, vol. 7, no. 6, pp. 631–640, Jun. 2014.

[8] T. P. E. Lockie *et al.*, "Synergistic adaptations to exercise in the systemic and coronary circulations that underlie the warm-up angina phenomenon," *Circulation*, vol. 126, no. 22, pp. 2565–2674, Nov. 2012. [Online]. Available: http://www.ncbi.nlm.nih.gov/pubmed/23124033

[9] K. N. Asrress *et al.*, "A unravelling the mechanisms of exercise induced ischaemia, its optimal assessment, and alleviation with nitroglycerine," *Heart*, vol. 100, no. Suppl 3, pp. A124–A125, May 2014.

[10] K. De Silva *et al.*, "Coronary wave energy: A novel predictor of functional recovery after myocardial infarction," *Circulation. Cardiovascular Interventions*, vol. 6, no. 2, pp. 166–175, Mar. 2013.

[11] S. Rivolo *et al.*, "Enhancing coronary wave intensity analysis robustness by high order central finite differences," *Artery Res.*, vol. 8, no. 3, pp. 98–109, 2014.

[12] S. Rivolo *et al.*, "Automatic selection of optimal Savitzky-Golay filter parameters for coronary wave intensity analysis," in *Proc. 36th Annu. Int. Conf. IEEE Eng. Med. Biol. Soc.*, Aug. 2014, pp. 5056–5059.
[13] M. C. Rolandi *et al.*, "Coronary wave intensity during the Valsalva manoeuvre in humans reflects altered intramural vessel compression responsible for extravascular resistance," *J. Physiol.*, vol. 590, no. Pt 18, pp. 4623–4635, Sep. 2012.
[14] M. C. Rolandi *et al.*, "Wave speed in human coronary arteries is not influenced by microvascular vasodilation: Implications for wave intensity analysis," *Basic Res. Cardiol.*, vol. 109, no. 2, p. 405, Mar. 2014.
[15] M. Siebes *et al.*, "Potential and limitations of wave intensity analysis in coronary arteries," *Med. Biol. Eng. Comput.*, vol. 47, no. 2, pp. 233–239, Feb. 2009.
[16] A. Savitzky and M. J. E. Golay, "Smoothing and differentiation of data by simplified least squares procedures." *Analytical Chem.*, vol. 36, no. 8, pp. 1627–1639, Jul. 1964.
[17] M. J. Kern *et al.*, "Physiological assessment of coronary artery disease in the cardiac catheterization laboratory: A scientific statement from the American Heart Association Committee on Diagnostic and Interventional Cardiac Catheterization, Council on Clinical Cardiology," *Circulation*, vol. 114, no. 12, pp. 1321–1341, Sep. 2006. [Online]. Available: http://www.ncbi.nlm.nih.gov/pubmed/16940193
[18] M. Siebes *et al.*, "Single-wire pressure and flow velocity measurement to quantify coronary stenosis hemodynamics and effects of percutaneous interventions," *Circulation*, vol. 109, no. 6, pp. 756–762, Feb. 2004. [Online]. Available: http://www.ncbi.nlm.nih.gov/pubmed/14970112
[19] J. Lee *et al.*, "Multiscale modelling of cardiac perfusion," in *Modeling the Heart and the Circulatory System*. New York, NY, USA: Springer, 2015, p. 300.
[20] J. Luo *et al.*, "Properties of Savitzky-Golay digital differentiators," *Digital Signal Process.*, vol. 15, pp. 122–136, 2005.
[21] M. U. A. Bromba and H. Ziegler, "Application hints for Savitzky-Golay digital smoothing filters," *Analytical Chem.*, vol. 53, no. 11, pp. 1583–1586, Sep. 1981. [Online]. Available: http://pubs.acs.org/doi/abs/10.1021/ac00234a011
[22] W. H. Press *et al.*, *Numerical Recipes in C (2nd ed.): The Art of Scientific Computing*, vol. 29. Cambridge, U.K.: Cambridge Univ. Press, 1992. [Online]. Available: http://www.jstor.org/stable/1269484?origin=crossref
[23] P.-O. Persson and G. Strang, *Smoothing by Savitzky-Golay and Legendre Filters* (ser. The IMA Volumes in Mathematics and its Applications), vol. 134. New York, NY, USA: Springer, 2003.
[24] S. R. Krishnan and C. S. Seelamantula, "On the selection of optimum Savitzky-Golay filters," *IEEE Trans. Signal Process.*, vol. 61, no. 2, pp. 380–391, Jan. 2013.
[25] C. M. Stein, "Estimation of the mean of a multivariate normal distribution," *Ann. Statist.*, vol. 9, no. 6, pp. 1135–1151, Nov. 1981.
[26] N. R. Gaddum *et al.*, "A technical assessment of pulse wave velocity algorithms applied to non-invasive arterial waveforms," *Ann. Biomed. Eng.*, vol. 41, pp. 2617–2629, 2013.
[27] J. E. Davies *et al.*, "Use of simultaneous pressure and velocity measurements to estimate arterial wave speed at a single site in humans," *Amer. J. Physiol. Heart Circulatory Physiol.*, vol. 290, no. 2, pp. H878–H885, Feb. 2006.

Authors' photographs and biographies not available at the time of publication.